

1 Supplementary material

2

3 **Novel CuCo_2O_4 Photonic Crystals for Optical Hydrogen Sensing:**

4 **Catalyst-Free Detection and Mechanistic Insights via in-situ Raman**

5 **Spectroscopy**

6 S Silpa^{1#}, Nidha Mariyam^{1#}, Kritika Sharu¹, Saptak Majumder¹, Joy Mitra¹, and Vinayak B

7 Kamble^{1,*}

8 ¹School of Physics, Indian Institute of Science Education and Research Thiruvananthapuram 695551 India.

9

10

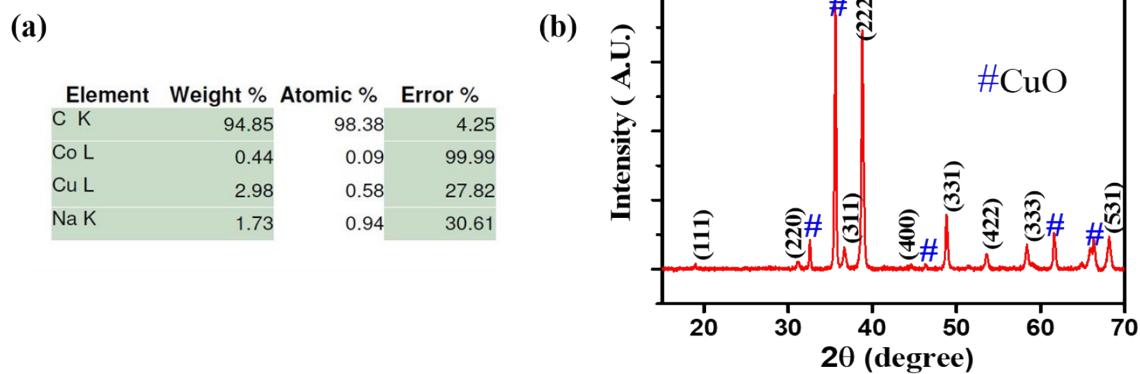


Figure S1: (a) Elemental percentages of CCO Opal thin film by SEM-EDS (b) XRD of synthesized CCO powder which was used to make a target for sputtering

11 **A. STRUCTURE AND COMPOSITION OF THE FILMS.**

12 Fig S1 (a) and (b) show the elemental percentage of the CCO opal thin film and the XRD pattern
 13 of the synthesized powder, respectively. A high percentage of carbon is attributed to the polymeric
 14 (Polystyrene) template, and Cu and Co are from CCO.

15

16

17

18

19

20 **B. PHOTONIC RESPONSE OF CCO OPAL FILMS AND ITS VARIATION WITH**
 21 **HYDROGEN GAS CONCENTRATION.**

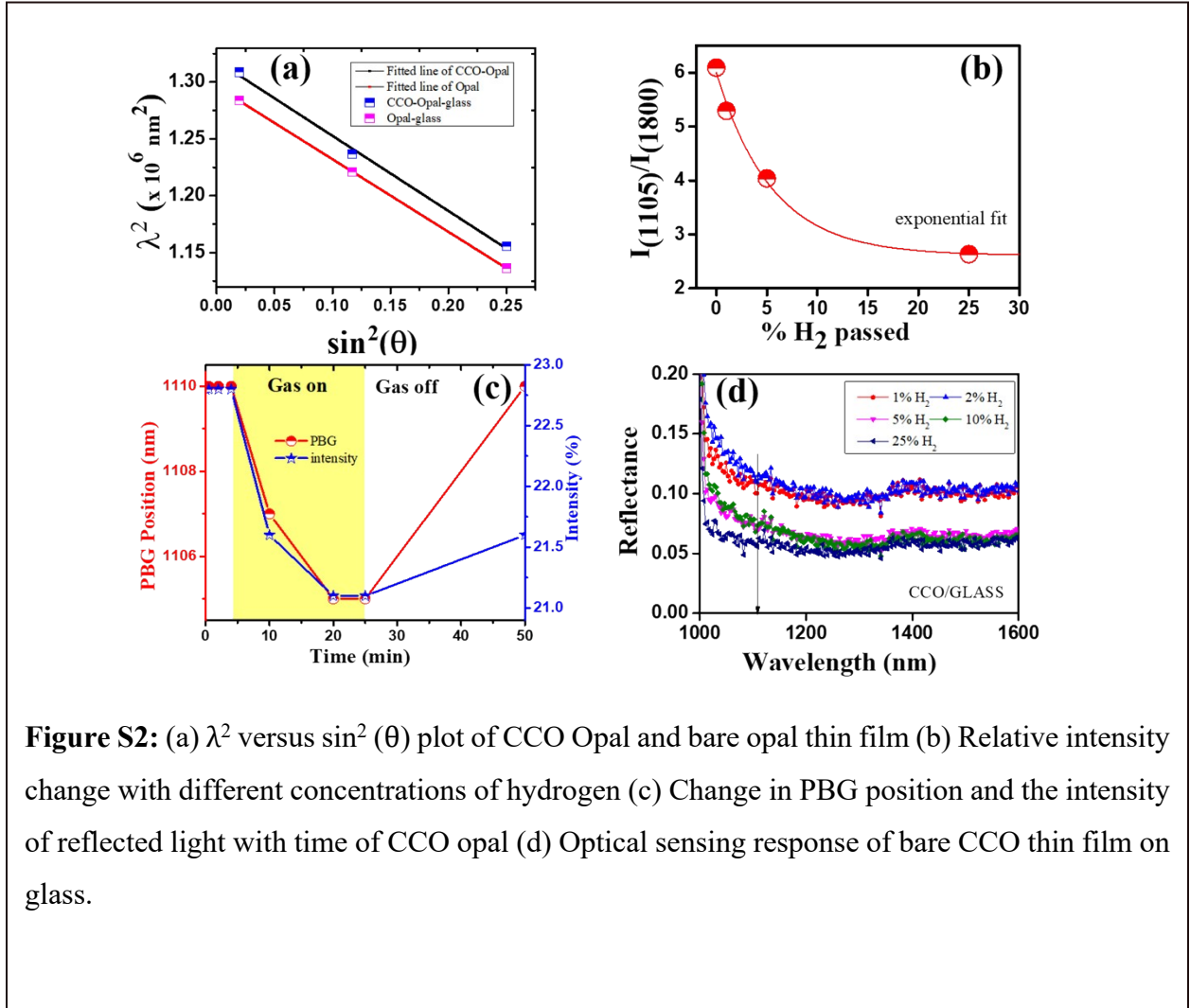


Figure S2: (a) λ^2 versus $\sin^2(\theta)$ plot of CCO Opal and bare opal thin film (b) Relative intensity change with different concentrations of hydrogen (c) Change in PBG position and the intensity of reflected light with time of CCO opal (d) Optical sensing response of bare CCO thin film on glass.

22

23 Fig S2(a) shows the λ^2 versus $\sin^2(\theta)$ using Bragg-Snell law for Opal on glass and
 24 Opal/glass. PBG positions of three incident angles were fitted with a linear function, and the slope
 25 and intercept were calculated to get the n_{eff} . Fig S2(b) shows the intensity ratio of reflected light
 26 at 1105 nm (PBG) and 1800 nm as a function of the concentration of hydrogen gas exposed. The
 27 intensity ratio decreases exponentially with the concentration. The instant change in PBG and
 28 intensity at PBG position with respect to time, as the hydrogen was exposed, were plotted in Fig

29 S2(c). The in-situ reflectance was taken for bare CCO, which is shown in Fig S2(d). Bare CCO
30 shows a very small decrease in intensity as the concentration was increased.

31

32 C. SEM AND RAMAN SPECTRUM OF CCO OPAL FILM.

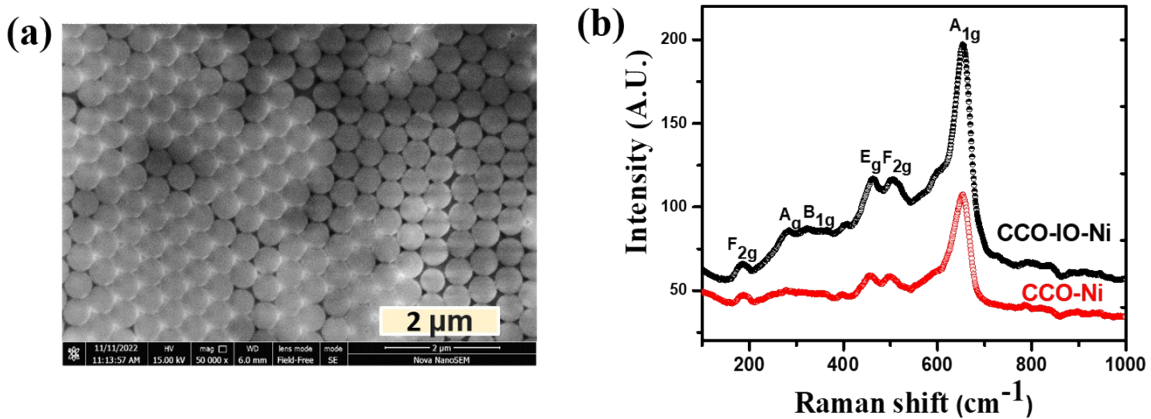


Figure S3: (a) SEM image of PS opal on nickel foil showing the necking between spheres after annealing (b) Raman Spectra of CCO-IO and bare CCO thin film on nickel foil.

33

34 Fig S3(a) shows the necked PS template used for PED to get CCO-IO. The spheres formed a
35 necking by annealing at a temperature. Fig S3(b) shows the Raman spectra of CCO-IO thin film
36 and CCO thin film. Both show several vibrations corresponding to different modes of CCO as well
37 as CuO, as mentioned in the plot.

38

39

40 **D. XPS STUDY OF CCO IO FILMS.**

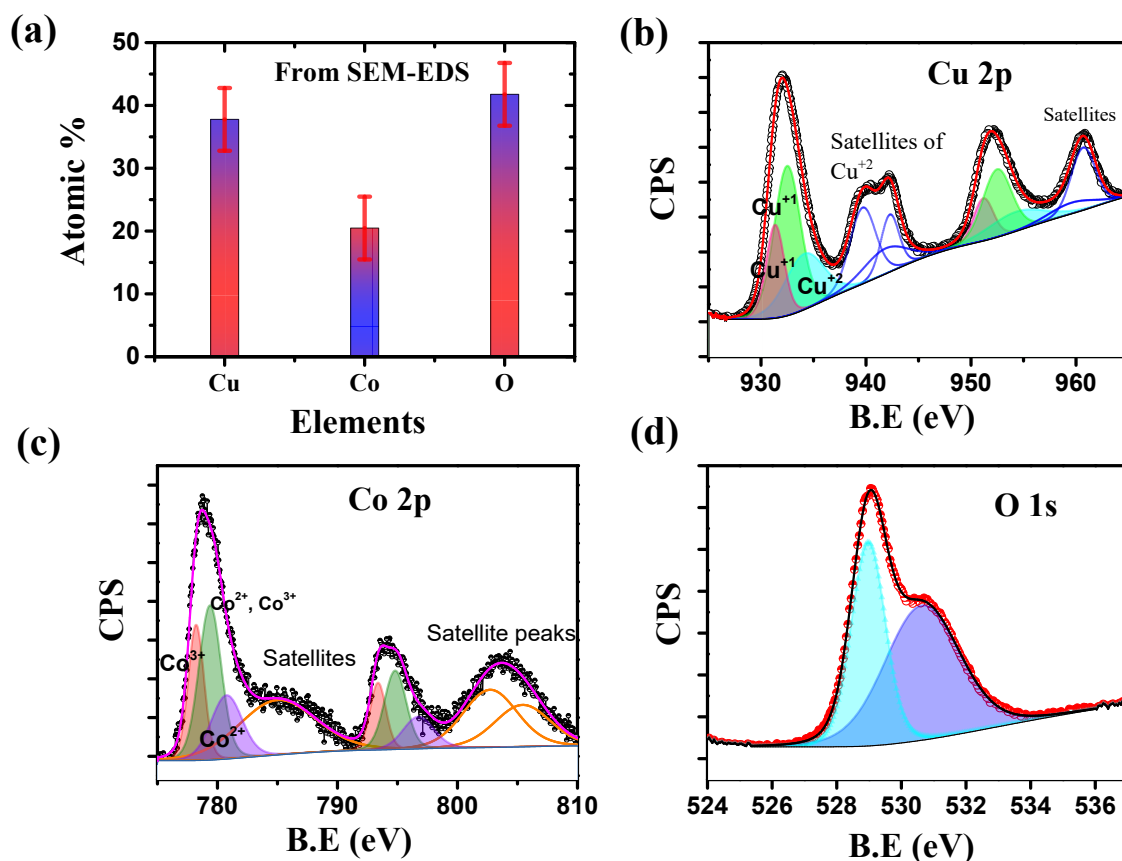


Figure S4: (a) Atomic percentages of each element from SEM-EDS of CCO IO, XPS spectra of (b) Cu 2p (c) Co 2p (d) O 1s of CCO-IO.

41

42 Fig S4 (a) shows the atomic percentages of each element of CCO-IO from SEM-EDS analysis.
 43 From the chemical formula for the spinel compound CuCo_2O_4 , it is expected that typical Cu: Co
 44 would have a 1:2 ratio. The excess Cu, in that case, is ascribed to the secondary phase of CuO,
 45 which was confirmed by the XRD and Raman spectra.

46 To further probe the material crystal structure and the chemical composition, XPS analysis
 47 was done for CCO-IO. The core-level spectra of Cu 2p, Co 2p, and O 1s are given in Fig S4 (a),

48 (b), and (c), respectively. Also, table S1 represents the peak maxima of Cu, Co, and O core level
49 resolved spectra.

50

51 Table S1. The XPS peak assignments in Cu, Co, and O core level resolved spectra.

Core level	Binding energy (eV)	Peak assignment
Cu 2p	931.3	octahedral Cu ⁺
	932.5	tetrahedral Cu ⁺
	934.1	octahedral Cu ²⁺ ,
Co 2p	778.1	octahedral Co ³⁺
	780.8	tetrahedral Co ²⁺
	779.6	mixed formation of Co ³⁺ and Co ²⁺
O 1s	528.9	O ²⁻ ion
	530.6	chemisorbed oxygen and lattice defects

52

53

54

55

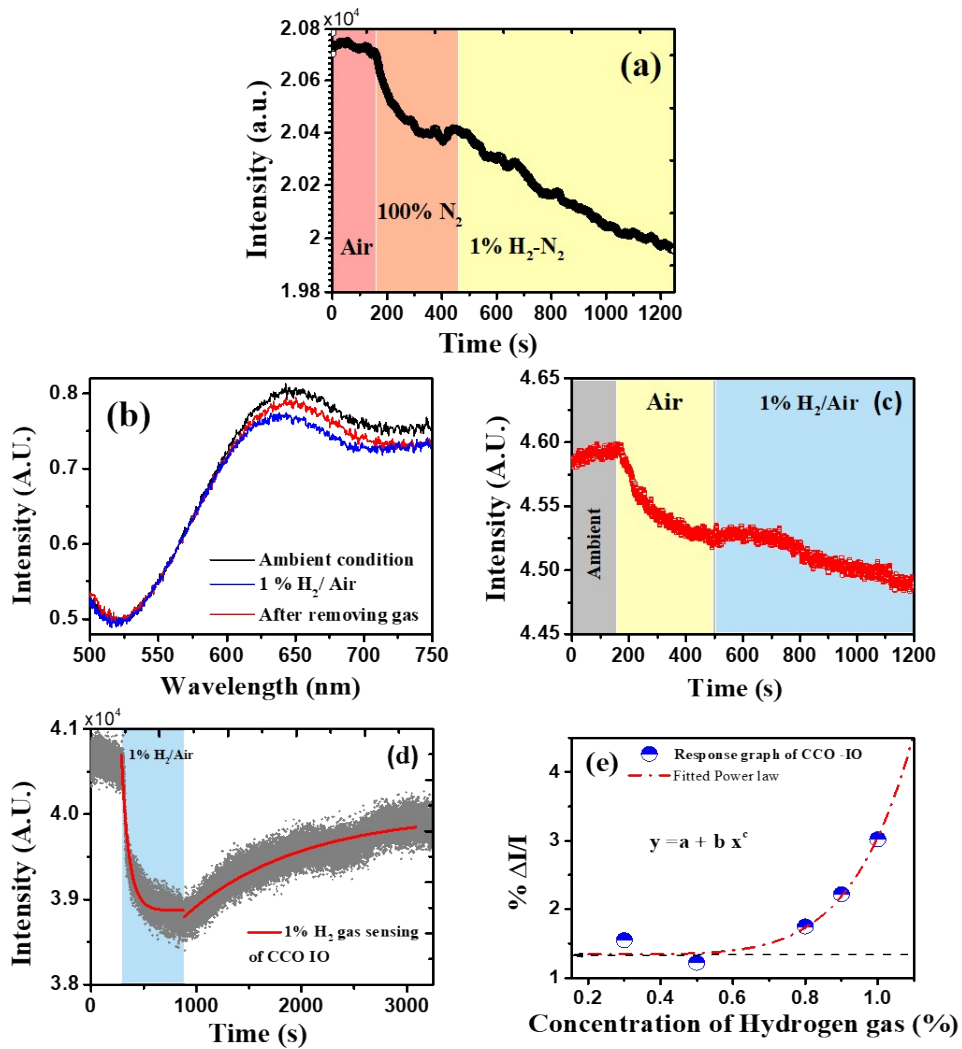


Figure S5: (a) Change in intensity of reflected light over time for 1% H₂ (b) in-situ reflectance spectra of CCO-IO with the exposure and recovery of 1% H₂-Air (c) Response curve of CCO-IO where 1% H₂-Air was exposed after passing Air for some time (d) Response and recovery of CCO-IO with exposing 1% H₂-Air from ambient conditions (e) Response curve of CCO IO fitted with power law towards different hydrogen gas concentrations.

58 The change in PBG position and intensity was observed when the sample was exposed to 1% H₂-
59 N₂ in ambient conditions. The response of CCO-IO in the presence of 1%H₂-N₂ and 1%H₂-Air is
60 plotted in Fig S5. Fig S5(a) shows the intensity change of CCO in the presence of 1% H₂-N₂ after
61 passing 100% N₂. Once the intensity was saturated in the presence of 100%N₂, 1%H₂-N₂ was
62 passed, where it decreased further.

63 In Fig S5(b), the in-situ reflectance shows the PBG change in the presence of hydrogen. Also, the
64 recovery of PBG position is visible. The intensity change with the exposure of hydrogen was
65 monitored with and without passing the carrier gas previously and plotted in Fig S5(c) and (d),
66 respectively. Fig S5(d) also shows the recovery of CCO-IO from hydrogen, and it is found to be
67 around 30 min. In the presence of 1%H₂-Air, the response increased with the concentration, as
68 shown in Fig S5(e). Here, it was fitted using power law.

69

70

71 Fig S6 shows the repeatability and selectivity of CCO-IO. The PBG shift of 12 ± 2 nm in the
72 presence of hydrogen gas was consistent over 200 days, which can be seen in Fig S6(a). This
73 confirms the repetitive sensing response of CCO-IO towards hydrogen gas. The selectivity of the
74 sensor towards hydrogen was confirmed by measuring the response towards other reducing gases,

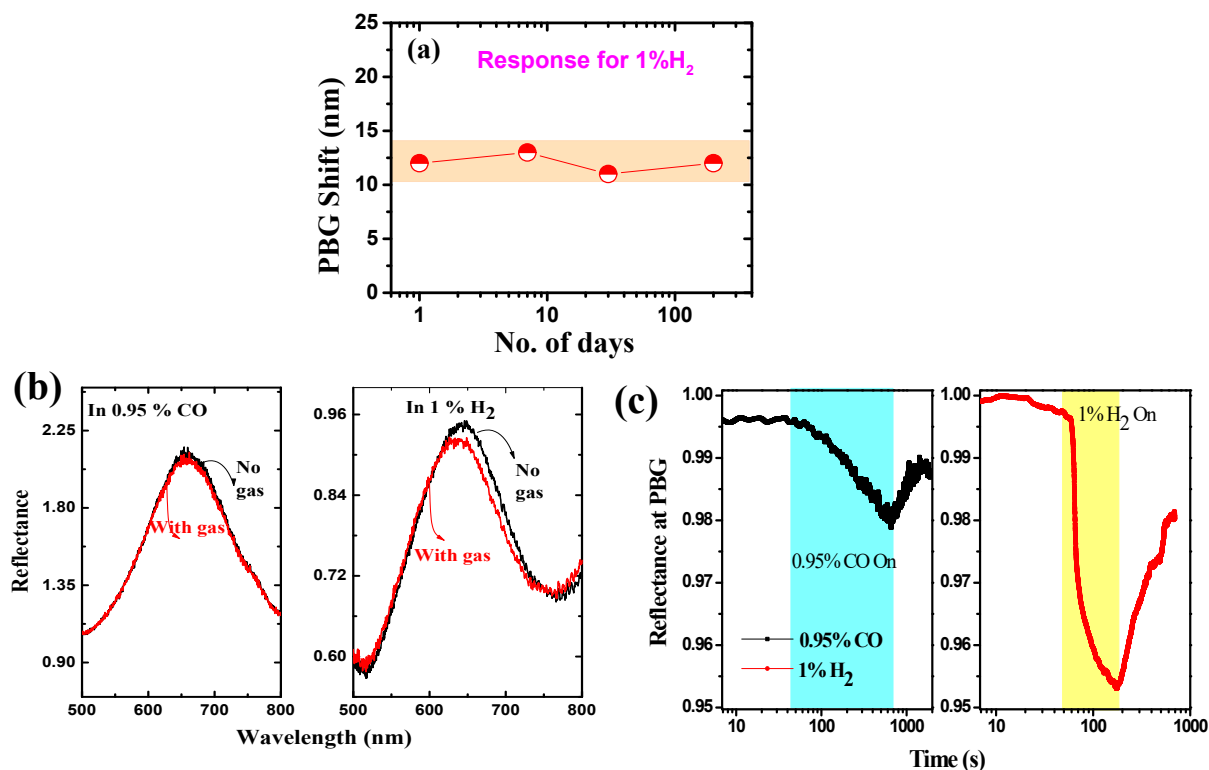


Figure S6: (a) Repeatability of the response of CCO-IO towards 1%H₂ over days (b) in-situ reflectance spectra of CCO-IO in the presence of 0.95% CO as compared with 1% H₂ (c) The dynamic change in reflectance while exposed to both 0.95% CO and 1% H₂ at PBG wavelength.

75 such as carbon monoxide (CO). As shown in Fig S6(b), no significant shift in PBG was observed
76 in the presence of CO. The intensity change was also less compared to hydrogen, which is shown
77 in Fig S6 (c).

78 F. IN-SITU RAMAN SPECTRA OF CCO-IO FILMS IN DIFFERENT ATMOSPHERES

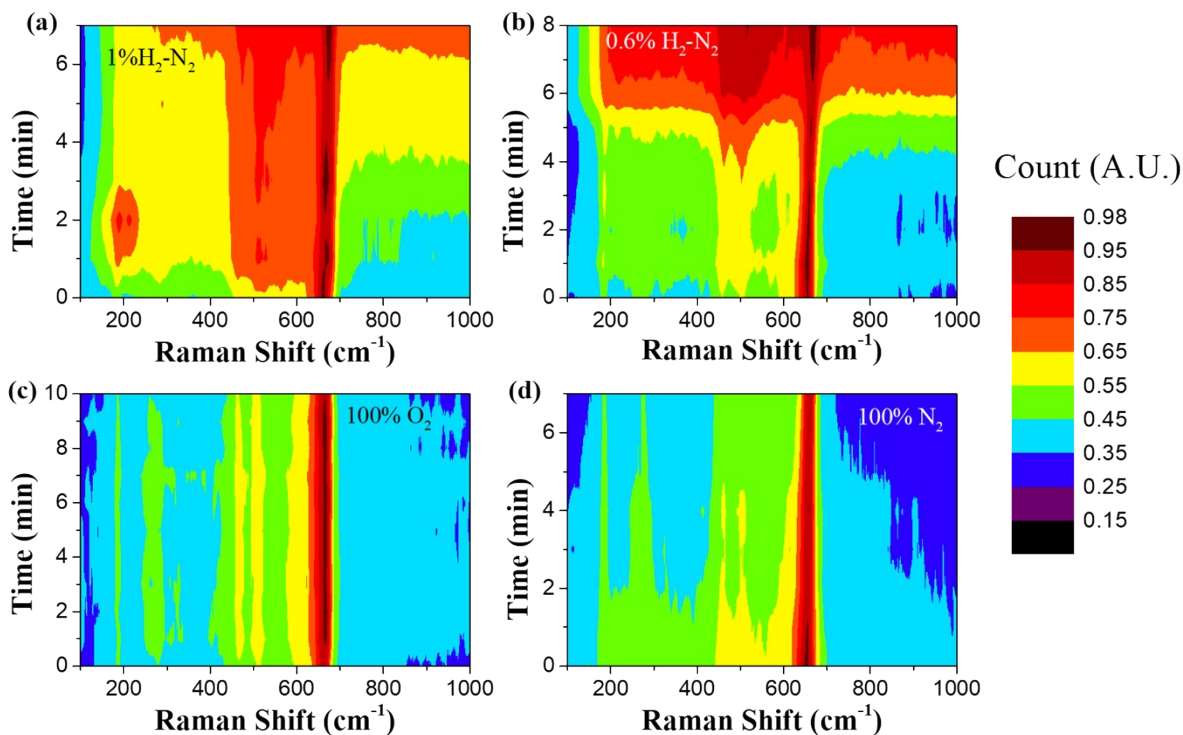


Figure S7: Contour Plots of in-situ Raman spectroscopy done in the presence of (a) 1% H₂-N₂, (b) 0.6% H₂-N₂, (c) 100% O₂, and (d) 100% N₂.

79

80 Contour plots of in-situ Raman spectra in the presence of 1% H₂-N₂, 0.6% H₂-N₂, 100% O₂, and
81 100% N₂ were plotted in Fig S7. The intensity of Raman peaks changed in the presence of 1% H₂-
82 N₂ and 0.6% H₂-N₂ but not in the presence of 100% O₂ and 100% N₂.